2019 American Control Conference (ACC)
Philadelphia, PA, USA, July 10-12, 2019

Relating global and local stochastic receptivity analysis of boundary layer flows

Wei Ran, Armin Zare, M. J. Philipp Hack, and Mihailo R. Jovanović

Abstract— **We utilize control-theoretic tools to study the receptivity of pre-transitional boundary layers to persistent stochastic excitation sources. White-in-time stochastic excitation is used to model the effect of free-stream turbulence on the linearized Navier-Stokes dynamics. We discuss similarities and differences resulting from local and global approaches in terms of steady-state energy amplification of velocity fluctuations and the underlying flow structures. While parallel flow analysis predicts a flow response that is dominated by the principal eigenmode of the covariance matrix, we show that global analysis yields subordinate eigenmodes that have nearly equal energetic contributions to that of the principal mode. We investigate this observation and provide a possible explanation for the disparity between the results of local and global receptivity analysis in spatially evolving flows.**

Index Terms— **Boundary layers, boundary layer receptivity, distributed systems, energy amplification, low-complexity modeling, Navier-Stokes equations, spatially evolving flows.**

I. Introduction

The receptivity of boundary layers to external excitation sources, e.g., free-stream turbulence, plays an important role in the laminar-turbulent transition process. External sources of excitation perturb the laminar velocity field and provide a pathway for the growth of small-amplitude perturbations to critical levels. While nonlinear dynamical models that are based on the Navier-Stokes (NS) equations provide insight into receptivity mechanisms, their implementation typically involves a large number of degrees of freedom and it ultimately requires direct simulation. This motivates the development of low-complexity models that are better suited for analysis, optimization, and flow control design.

The linearized NS equations have been widely used for modal and non-modal stability analysis of both parallel and non-parallel flows [1], [2]. In particular, the linearized NS equations subject to stochastic excitation have been successfully employed to replicate structural and statistical features of both transitional [3]–[5] and turbulent [6]–[8] shear flows. However, most previous studies have focused on parallel flow configurations and linearized models around mean profiles that are invariant in two spatial directions. For example in channel flows, translational invariance allows for the decoupling of the dynamical equations across streamwise and spanwise wavenumbers via Fourier transform, resulting in significant computational advantage.

On the other hand, in the flat-plate boundary layer, streamwise and wall-normal inhomogeneity require discretization in two spatial dimensions and thus lead to models of significantly larger sizes. As a result, modal and non-modal analyses in spatially evolving flows are significantly more challenging than in parallel flows. However, due to the slowly varying nature of boundary layer flows at sufficiently large Reynolds numbers, parallel flow assumptions have provided the means for the development of simplified models that capture the spatial evolution of modes within the boundary layer [1], [9]–[11]. While this assumption offers significant computational advantage, it does not account for the effect of the spatially evolving base flow on the stability of the boundary layer. Global stability analysis addresses this issue by accounting for the spatially varying nature of the base flow and discretizing spatially inhomogeneous dimensions. Previously, tools from sparse linear algebra in conjunction with iterative schemes have been employed to conduct modal [12], [13] and non-modal [14]–[16] analyses in spatially evolving flows.

Herein, we study the receptivity of the boundary layer flow to exogenous excitation which we model as a persistent white-in-time stochastic forcing entering in the immediate vicinity of the wall. We solve the algebraic Lyapunov equation to obtain the steady-state response of the flow and compare and contrast results obtained under the parallel flow assumption with those of global analysis. Our simulation-free approach enables the computationally efficient assessment of the energy spectrum of spatially evolving flows, without relying on a particular form of inflow conditions or computation of the full spectrum of the linearized dynamical generator.

Our presentation is organized as follows. In Section II, we introduce the stochastically forced linearized NS equations and describe the tools that we use to compute the steady-state response and energy amplification of velocity fluctuations. In Section III, we present results from locally parallel and global receptivity analyses of the Blasius boundary layer flow. In Section IV, we examined the flow structures that are extracted from steady-state covariance matrices. In Section V, we provide a discussion on the origin of disparity between locally parallel and global results. Finally, we present concluding thoughts in Section VI.

Financial support from the Air Force Office of Scientific Research under Awards FA9550-16-1-0009 and FA9550-18-1-0422 is gratefully acknowledged.

Wei Ran is with the Department of Aerospace and Mechanical Engineering, University of Southern California, Los Angeles, CA 90089. Armin Zare and Mihailo R. Jovanović are with the Ming Hsieh Department of Electrical and Computer Engineering, University of Southern California, Los Angeles, CA 90089. M. J. Philipp Hack is with the Center for Turbulence Research, Stanford University, Stanford, CA 94305. E-mails: wran@usc.edu, armin.zare@usc.edu, philipp.hack@stanford.edu, mihailo@usc.edu.

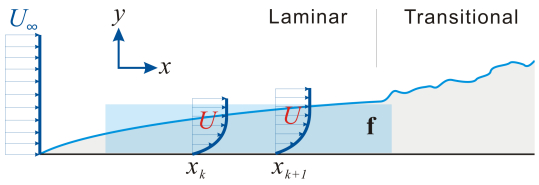

Fig. 1. Geometry of transitional boundary layer flow with stochastic excitation $\mathbf{f}$ entering in the blue shaded region.

II. Stochastically forced linearized model

For incompressible Newtonian fluid flow, the linearized NS equations around a two-dimensional base flow profile $\bar{\mathbf{u}} = [\,U(x,y)\;\; V(x,y)\;\; 0\,]^T$ are given by

$$\begin{aligned} \mathbf{v}_t &= -(\nabla\cdot\bar{\mathbf{u}})\,\mathbf{v} - (\nabla\cdot\mathbf{v})\,\bar{\mathbf{u}} - \nabla p + \frac{1}{Re_0}\Delta\mathbf{v} + \mathbf{f} \\ 0 &= \nabla\cdot\mathbf{v} \end{aligned} \tag{1}$$

where $\mathbf{v} = [\,u\;\; v\;\; w\,]^T$ is the vector of velocity fluctuations, u, v, and w are components of the fluctuating velocity field in the streamwise (x), wall-normal (y), and spanwise (z) directions, p denotes pressure fluctuations, and $\mathbf{f}$ is an additive zero-mean stochastic body forcing. As shown in Fig. 1, the external excitation of the boundary layer flow can enter in various wall-normal regions. The Reynolds number $Re_0 = U_\infty\delta_0/\nu$ is defined based on the Blasius length-scale $\delta_0 = \sqrt{\nu\,x_0/U_\infty}$, in which x_0 is the initial streamwise location which denotes the distance from the leading edge, U_∞ is the free-stream velocity, and ν is the kinematic viscosity. The local Reynolds number Re at distance x from the reference point x_0 is given by $Re = Re_0\sqrt{1+x/x_0}$. Velocities are non-dimensionalized by U_∞, time by δ_0/U_∞, and pressure by ρU_∞^2, where ρ is the fluid density.

By eliminating pressure, the linearized equations (1) can be brought to the evolution form

$$\begin{aligned} \boldsymbol{\varphi}_t(x,y,k_z,t) &= [\mathbf{A}(k_z)\,\boldsymbol{\varphi}(\cdot,k_z,t)](x,y) + \\ &\quad [\mathbf{B}(k_z)\,\mathbf{f}(\cdot,k_z,t)](x,y) \\ \mathbf{v}(x,y,k_z,t) &= [\mathbf{C}(k_z)\,\boldsymbol{\varphi}(\cdot,k_z,t)](x,y) \end{aligned} \tag{2}$$

where the state $\boldsymbol{\varphi} = [\,v\;\; \eta\,]^T$ contains wall-normal velocity v and vorticity $\eta = \partial_z u - \partial_x w$ components of the fluctuation field [1]. Here, homogeneity of the base flow in z has allowed for the parameterization of the evolution model (2) over various spanwise wavenumbers k_z via spatial Fourier transform. A detailed description of operators $\mathbf{A}$, $\mathbf{B}$, and $\mathbf{C}$ in (2) can be found in [17, Appendix A]. Note that a wall-parallel base flow assumption in the form of $\bar{\mathbf{u}} = [\,U(y)\;\; 0\;\; 0\,]^T$ allows for an additional parameterization of the dynamics over streamwise wavenumbers k_x, resulting in

$$\begin{aligned} \boldsymbol{\varphi}_t(k_x,y,k_z,t) &= [\mathbf{A}(k_x,k_z)\,\boldsymbol{\varphi}(\cdot,k_x,k_z,t)](y) + \\ &\quad [\mathbf{B}(k_x,k_z)\,\mathbf{f}(\cdot,k_x,k_z,t)](y) \\ \mathbf{v}(k_x,y,k_z,t) &= [\mathbf{C}(k_x,k_z)\,\boldsymbol{\varphi}(\cdot,k_x,k_z,t)](y) \end{aligned} \tag{3}$$

Finite-dimensional approximations of the operators in Eqs. (2) and (3) in the non-homogeneous directions yields

$$\begin{aligned} \dot{\boldsymbol{\psi}}(t) &= A\,\boldsymbol{\psi}(t) + B\,\mathbf{f}(t) \\ \mathbf{v}(t) &= C\,\boldsymbol{\psi}(t) \end{aligned} \tag{4}$$

with $\boldsymbol{\psi}(t) \in \mathbb{C}^{2N_xN_y}$ and $\mathbf{v}(t) \in \mathbb{C}^{3N_xN_y}$ for global flow analysis (when the streamwise direction is non-homogeneous), and $\boldsymbol{\psi}(t) \in \mathbb{C}^{2N_y}$ and $\mathbf{v}(t) \in \mathbb{C}^{3N_y}$ for parallel flow analysis.

A. Energy amplification to stochastic excitation

In statistical steady-state, the covariance matrices of the state and output in Eqs. (4),

$$X := \lim_{t\to\infty} \mathbf{E}\,(\boldsymbol{\psi}(t)\,\boldsymbol{\psi}^*(t))$$

and

$$\Phi := \lim_{t\to\infty} \mathbf{E}\,(\mathbf{v}(t)\,\mathbf{v}^*(t))$$

are related as:

$$\Phi = C\,X\,C^*. \tag{5}$$

Here, $\mathbf{E}(\cdot)$ is the expectation operator and the superscript $*$ denotes complex conjugate transpose. The matrix Φ contains information about all second-order statistics of the fluctuating velocity field, including the Reynolds stresses.

We assume that $\mathbf{f}(t)$ in Eq. (4) is zero-mean and white-in-time with spatial covariance matrix $W = W^*$, i.e,

$$\langle \mathbf{f}(t_1)\,\mathbf{f}^*(t_2)\rangle = W\,\delta(t_1 - t_2) \tag{6}$$

where δ is the Dirac delta function. At subcritical Reynolds numbers, for which the dynamical generator A is stable, the steady-state covariance X of the state $\boldsymbol{\psi}(t)$ can be determined as the solution to the algebraic Lyapunov equation

$$A\,X + X\,A^* = -B\,W\,B^*. \tag{7}$$

The energy amplification of stochastically-forced flow can be computed from the solution to this equations as:

$$E = \mathrm{trace}\,(C\,X\,C^*) \tag{8}$$

To specify the wall-normal extent of forcing, we define $\mathbf{f} := f(y)\mathbf{f}_s$ where $\mathbf{f}_s$ represents white solenoidal forcing and $f(y)$ is a smooth filter function defined as

$$f(y) := \frac{1}{\pi}\left(\mathrm{atan}(y - y_1) - \mathrm{atan}(y - y_2)\right). \tag{9}$$

Here, y_1 and y_2 determine the region in which the forcing $\mathbf{f}$ will be concentrated.

B. Numerical setup

We study the energy amplification of velocity fluctuations around the Blasius boundary layer profile with $Re_0 = 232$ and use the local Blasius length-scale as the unit length, i.e. $\delta_0 = 1$. White-in-time stochastic forcing of unit variance ($W = I$) is assumed to enter in the immediate vicinity of the wall ($y_1 = 0$ and $y_2 = 5$ in Eq. (9)).

In what follows we first consider the base flow to be parallel (cf. Eqs. (3)) and discretize the operators over a

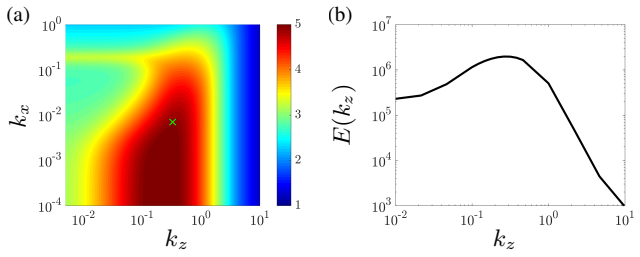

Fig. 2. (a) Plot of $\log_{10}(E(k_x, k_z))$ in the parallel Blasius boundary layer flow with $Re_0 = 232$ subject to white-in-time stochastic excitation entering in the vicinity of the wall. The green cross corresponds to the wavenumber pair of streaks. (b) Energy amplification of velocity fluctuations due to near-wall forcing resulting from global flow analysis, which involves linearization around a spatially varying Blasius profile with $Re_0 = 232$.

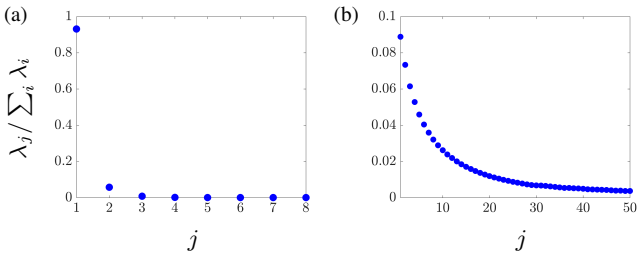

Fig. 3. Contribution of various eigenvalues of the velocity covariance matrix Φ of the Blasius boundary layer flow with $Re_0 = 232$ subject to wall-attached white-in-time stochastic forcing resulting from (a) parallel flow analysis at $(k_x, k_z) = (7 \times 10^{-3}, 0.33)$, and (b) global flow analysis at $k_z = 0.32$.

wall-normal domain of $L_y = 25$ using a pseudospectral discretization scheme with $N_y = 100$ Chebyshev collocation points [18]. Homogenous Dirichlet boundary conditions are imposed on wall-normal vorticity, and Dirichlet/Neumann boundary conditions are imposed on wall-normal velocity. We use 50×51 logarithmically spaced wavenumbers with $k_x \in [10^{-4}, 1]$ and $k_z \in [5 \times 10^{-3}, 10]$ to parameterize the linearized NS equations in the homogeneous directions.

In contrast to the parallel flow model, the global model based on the discretization of (2) involves a larger number of states due to the non-homogeneous streamwise direction. We consider $N_x = 100$ and $N_y = 50$ collocations points over the streamwise and wall-normal domains of length $L_x = 900$ and $L_y = 25$. In both parallel and global analyses, grid convergence has been verified by doubling the number of points used in discretizing the differential operators.

Similar to the parallel flow setup, we enforce homogenous Dirichlet and homogeneous Dirichlet/Neumann boundary conditions in the wall-normal direction for η and v, respectively. At the inflow, we impose homogeneous Dirichlet boundary conditions on η, i.e., $\eta(0, y) = 0$, and homogeneous Dirichlet/Neumann boundary conditions on v, i.e., $v(0, y) = v_y(0, y) = 0$. Finally, the outflow boundary conditions for both state variables and the streamwise derivative of the wall-normal component (v_x) are determined via linear extrapolation [19]. Moreover, we introduce sponge layers in the streamwise direction to mitigate the influence of boundary conditions on the fluctuation dynamics within the computational domain [13], [20]; see [21] for additional details.

III. Energy Spectrum of Velocity Fluctuations

We first examine energy amplification of velocity fluctuations subject to stochastic forcing under the locally parallel flow assumption. In this case, the evolution model is parameterized over various horizontal wavenumber pairs (k_x, k_z), which reduces the computational complexity of obtaining the energy spectrum. Figure 2(a) shows the energy spectrum of velocity fluctuations subject to wall-attached stochastic forcing. The energy of velocity fluctuations is most amplified at low streamwise wavenumbers ($k_x \approx 0$) with a global peak at $k_z \approx 0.25$. This indicates that streamwise elongated streaks are the dominant flow structures that result from persistent stochastic excitation of the boundary layer flow. In addition to streaks, the energy spectrum shown in Fig. 2(a) also predicts the emergence of Tollmien-Schlichting (TS) waves at $k_x \approx 0.19$. Both streaks and TS waves have been previously observed in experimental studies [22].

On the other hand, the evolution model considered in global flow analysis is only parameterized over spanwise wavenumbers, and as a result, the corresponding Lyapunov equations are of appreciably higher dimensionality. Figure 2(b) shows the k_z-dependence of the energy amplification for stochastic excitation entering in the immediate vicinity of the wall. The largest energy amplification is observed for $k_z = 0.32$, which is again consistent with previous numerical studies on the receptivity to free-stream turbulence [23], [24].

While the energy amplification reported in Fig. 2 is determined by summation over all eigenvalues of the output covariance matrix Φ (cf. (8)), it is also instructive to examine the contribution of individual eigenmodes. Figure 3(a) shows the contribution of the first 8 eigenvalues of Φ resulting from parallel flow analysis at $(k_x, k_z) = (7 \times 10^{-3}, 0.33)$ (green cross in Fig. 2(a)). The principal mode which corresponds to the largest eigenvalue, contains approximately 93% of the total energy. Figure 3(b) shows the contribution of the first 50 eigenvalues of the output velocity covariance matrix Φ resulting from global flow analysis at $k_z = 0.32$ (peak of the energy curve in Fig. 2(b)). Here, we observe that in contrast to the parallel flow analysis, other eigenvalues play a more prominent role. This implies that in global analysis the principal eigenmode of Φ cannot represent the full complexity of the spatially evolving flow. We expand on this aspect in the following sections.

IV. Flow Structures Extracted from the Steady-State Covariance Matrix

In this section, we examine the flow structures that can be extracted from various eigenmodes of Φ in Eq. 5, with X computed from Eq. (7). In both locally parallel and global flow analyses, symmetries in the homogeneous directions can

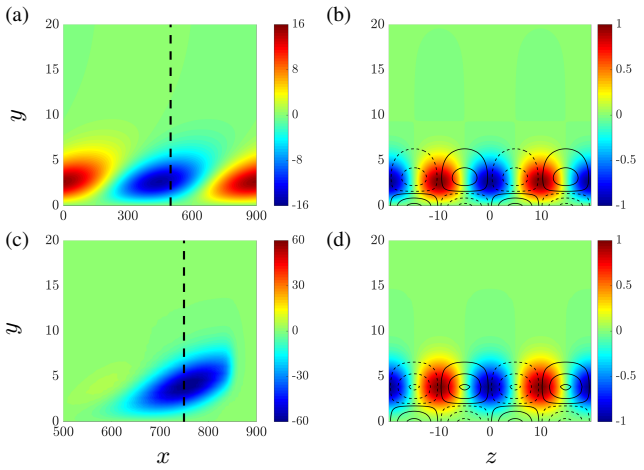

Fig. 4. Flow structures resulting from excitation of the boundary layer flow with $Re_0 = 232$ in the immediate vicinity of the wall extracted from the principal modes of the steady-state covariance matrix; (a,b) parallel flow analysis at $(k_x, k_z) = (7 \times 10^{-3}, 0.33)$; (c,d) global flow analysis at $k_z = 0.32$. (a) Streamwise velocity at $z = 0$. (b) y-z slice of streamwise velocity (colors) and vorticity (contour lines) at $x = 500$ corresponding to the cross-plane slice indicated by the dashed line in (a). (c) Streamwise velocity at $z = 0$. (d) y-z slice of streamwise velocity (colors) and vorticity (contour lines) at $x = 750$ corresponding to the dashed line in (c).

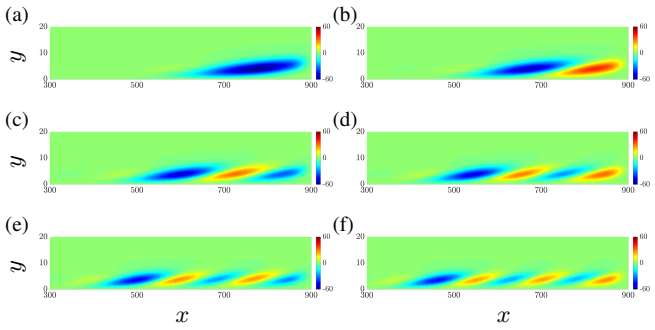

Fig. 5. Streamwise velocity at $z = 0$ corresponding to the first six eigenmodes of the steady-state covariance matrix Φ resulting from near-wall excitation of the boundary layer flow with $Re_0 = 232$ and at $k_z = 0.32$; (a) $j = 1$, (b) $j = 2$, (c) $j = 3$, (d) $j = 4$, (e) $j = 5$, and (f) $j = 6$ where j corresponds to ordering in Fig. 3(b).

be exploited to reconstruct flow structures and study their spatial extent; see [8, Eq. (5.4)].

As mentioned in the previous section, parallel flow analysis of the stochastically forced boundary layer flow predicts the dominant amplification of streamwise elongated flow structures. Figures 4(a) and 4(b) show the streamwise component of such flow structures corresponding to the principal eigenmode of the steady-state covariance matrix with $(k_x, k_z) = (7 \times 10^{-3}, 0.33)$. As shown in these figures, the streamwise elongated structures are situated between counter-rotating vortical motions in the cross-stream plane and contain alternating regions of fast- and slow-moving fluid, which are slightly inclined (and detached) relative to the wall. Even though these structures do not capture the full complexity of transitional flow, such alignment of counter-rotating vortices and streaks is closely related to the lift-up mechanism and the generation of streamwise elongated streaks that are studied via optimal growth analysis of boundary layer flow [24]–[27].

Although the principal eigenmode of Φ from global flow analysis cannot represent the full complexity of the spatially evolving flow, we examine its corresponding spatial structure to provide a comparison with the result of parallel flow analysis. Figure 4(c) shows the streamwise elongated structures of the streamwise component of the principal eigenmode of Φ resulting from near-wall stochastic forcing of the boundary layer flow with $k_z = 0.32$. The streamwise growth of the streaks can be observed. The cross-plane view of Fig. 4(d) shows that the resulting streaky structures are situated between counter-rotating vortical motions in the cross-stream plane and they contain alternating regions of fast- and slow-moving fluid that are slightly inclined to the wall. The similarity between the result of locally parallel and global analyses is evident from the colorplots of Fig. 4.

Suboptimal modes in global flow analysis

We proceed to examine the spatial structure of less energetic eigenmodes of Φ resulting from near-wall stochastic excitation of the boundary layer flow. As shown in Fig. 3(b), the first six eigenmodes respectively contain 8.9%, 7.3%, 6.1%, 5.3%, 4.6%, and 4.0% of the total energy of the flow. We again use the streamwise velocity component to study the spatial structure of the corresponding eigenmodes. As shown in Fig. 5(b), while the principal mode consists of a single streamwise-elongated streak, the second mode is comprised of two shorter high- and low-speed streaks. Similarly, the third and fourth modes respectively contain three and four streaks. These streaks become weaker and shorter in the streamwise direction and have alternating contributions to the velocity field; see Figs. 5(c) and 5(d). As the mode number increases, the streamwise extent of these structures further reduces. Moreover, they appear at an earlier streamwise location, and their peak value moves closer to the leading edge. This breakup into shorter streaks for higher modes is reminiscent of the dominant modes that are identified in parallel flow analysis for increasingly larger streamwise wavenumbers and at various streamwise locations (or Reynolds numbers). The fundamental spatial frequencies that are extracted from the streamwise variation of the eigenmodes of Φ using spatial Fourier transform in x (cf. Fig. 5) provide information about the streamwise length-scales of flow structures; see [17] for additional information.

V. Discussion

In this section, we seek an explanation for the differences between the results of locally parallel and global receptivity analyses. We first investigate the influence of a spatially evolving base flow on the steady-state response obtained from solving Eq. (7). For this purpose, we consider linearization around a parallel (streamwise invariant) boundary layer

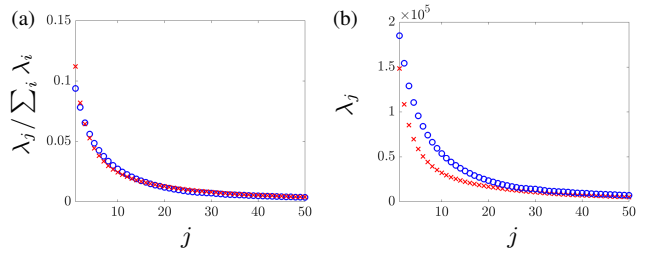

Fig. 6. The first 50 eigenvalues of the covariance matrix Φ corresponding to the dynamics (2) linearized around a parallel (red crosses) and spatially evolving (blue circles) Blasius boundary layer profile. Here, $Re_0 = 232$ and the spanwise wavenumber is $k_z = 0.32$. (a) Energetic contributions; (b) amplitudes.

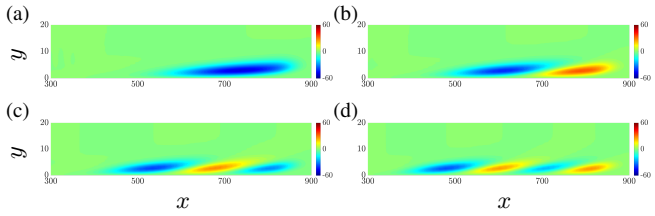

Fig. 7. Streamwise velocity at $z = 0$ corresponding to the first four eigenmodes of the steady-state covariance matrix Φ resulting from near-wall excitation of fluctuation dynamics (2) linearized around the parallel base flow at $Re_0 = 232$ with $k_z = 0.32$; (a) $j = 1$, (b) $j = 2$, (c) $j = 3$, (d) $j = 4$ where j corresponds to ordering in Fig. 6.

flow, but do not exploit the homogeneity of the dynamics in x and discretize the operators in the streamwise direction in the same way as in the wall-normal direction. Figure 6 illustrates the arrangement of eigenvalues of the covariance matrix Φ resulting from linearization around parallel and non-parallel base flow profiles. As shown in Fig. 6(a), when the base flow is assumed to be parallel, the primary eigenvalues retains a more significant portion of the total energy. Furthermore, Fig. 6(b) demonstrates how spatial evolution of the base flow can lead to increased energy amplification across all eigenmodes of the covariance matrix. On the other hand, as shown in Fig. 7, spatial visualization of various eigenmodes of Φ uncovers similar periodic flow structures to that of linearizing around a spatially evolving base flow (cf. Fig. 5). While the spatial evolution of the base flow plays an important role in distributing energy across various eigenmodes, it appears to have little effect on the shape of the amplified flow structures. Finally, we note that even in the presence of a spatially invariant base flow, spatial discretization of the streamwise dimension results in a full-rank covariance matrix Φ. This is in contrast to the result of parallel flow analysis (cf. Fig. 3(a)). We next provide an illustrative example to gain insight into the significance of subordinate eigenmodes of the covariance matrix resulting from spatial discretization of non-homogeneous directions.

An example: 2D diffusion equation

Consider a stochastically forced 2D diffusion equation

$$\xi_t \;=\; (\partial_{xx} \,+\, \partial_{yy})\,\xi \,+\, \mathbf{f} \qquad (10)$$

in which Dirichlet boundary conditions are imposed on the state ξ in both x and y directions and the size of the domain is given by L_x and L_y. The eigenvalues of the dynamical generator in (10) are

$$\lambda_{m,n} \;=\; -\left((m\pi/L_x)^2 \,+\, (n\pi/L_y)^2\right); \quad m,n \in \mathbb{Z}^+$$

and the corresponding eigenfunctions are sinusoids that include $m/2$ and $n/2$ periods in x and y directions, respectively. When the stochastic forcing is white-in-time with spatial covariance $W = I$, the steady-state covariance matrix $\Xi = \lim_{t\to\infty} \mathbf{E}\left(\xi(t)\,\xi^*(t)\right)$ can be expressed via the integral representation,

$$\Xi \;=\; \int_0^\infty \mathrm{e}^{At}\, W \mathrm{e}^{A^* t}\, \mathrm{d}t$$

where e^{At} is the strongly-continuous semi-group generated by $A := \partial_{xx} + \partial_{yy}$ with proper boundary conditions. Since A is normal, the expression for Ξ can be simplified to

$$\Xi \;=\; G\,\mathrm{diag}\{-\frac{1}{2\lambda_{m,n}}\}\,G^* \qquad (11)$$

where G contains orthonormal eigenfunctions of A that are weighted according to the eigenvalues $-1/(2\,\lambda_{m,n})$.

We emulate a boundary layer configuration, by considering a stretched spatial domain with $L_x = 20$ and $L_y = 2$ and use 50 Chebyshev collocation points to discretize in y. Figure 8 shows the energy distribution of various eigenmodes of the covariance matrix Ξ for two instances that differ in the application of Fourier transform in the x. When the equations are parameterized over wavenumbers k_x, the covariance matrix Ξ retains a dominant principal mode (Fig. 8(a)). For $k_x = \pi/20$, the eigenvalues of Ξ are given by $\frac{1}{2}\left((\pi/20)^2 + (n\pi/2)^2\right)^{-1}$, and they decrease at an approximate rate of $1/(n\pi)^2$, thereby resulting in the dominance of the principal eigenmode. In contrast, when the homogeneity in x is not exploited, a global approach, which discretizes the x dimension in the same way as y, results in a covariance matrix Ξ that is *not* low-rank (Fig. 8(b)). This approach yields eigenvalues of the form $\frac{1}{2}\left((m\pi/20)^2 + (n\pi/2)^2\right)^{-1}$. Because of the stretched domain ($L_x \gg L_y$), the eigenvalues initially decrease more gradually as their ordering in m precedes n. To illustrate the ordering of eigenfunctions, Fig. 9 shows the spatial structure of the 17th mode ($m = 17$, $n = 1$), which precedes the 18th mode ($m = 1$, $n = 2$). The eigenvalues corresponding to these modes are marked by red circles in Fig. 8(b). The first 17 modes are sinusoids that include $1/2$ period in y and respectively $1/2, \cdots, 17/2$ periods in x.

Remark 1: In boundary layer flow, the dynamical generator of the linearized NS equations (4) is non-normal, and as a result, the covariance matrix Φ cannot be expressed in a form similar to Eq. (11). Nevertheless, the eigenmodes of Φ inherit a periodic structure from a (non-trivially) weighted combination of spatially periodic eigenmodes of dynamical generator A. Furthermore, similar to the diffusion equation, the spatial domain that contains the shear of the boundary

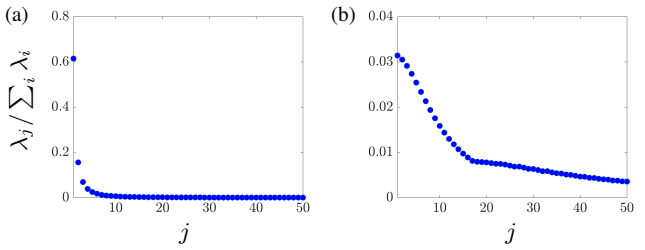

Fig. 8. Contribution of the first 50 eigenvalues of the covariance matrix Ξ resulting from (a) parameterization in the x direction ($k_x = \pi/20$), and (b) without parameterization in the x direction (global approach). Red circles mark the 17th and 18th eigenvalues.

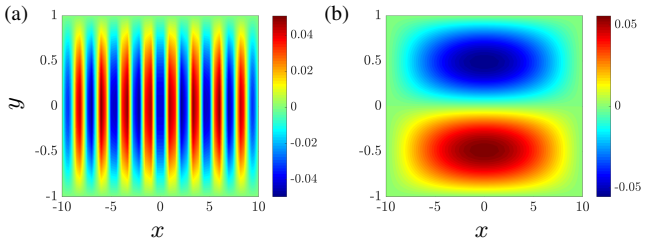

Fig. 9. The spatial structure of the 17th (a) and 18th (b) eigenfunctions of Ξ from a global approach that does not account for the homogeneity in x to parameterize the dynamics across Fourier modes.

layer flow is stretched in the streamwise direction ($L_x \gg L_y$) resulting in a gradually degrading eigenspectrum in Φ. A rigorous mathematical explanation requires further scrutiny and it is a topic of our ongoing research.

VI. Concluding Remarks

We study the energy amplification of Blasius boundary layer flow subject to white-in-time stochastic forcing using the linearized NS equations. The dynamics of flow fluctuations are captured by models that arise from locally parallel and global perspectives and energy amplification is quantified using the variance of the steady-state response from the algebraic Lyapunov equation. Our findings demonstrate good agreement between the results obtained from parallel and global flow models. The outcome establishes the efficacy of using parallel flow assumptions in the receptivity analysis of boundary layer flows, especially when it is desired to evaluate the energetic contribution of individual streamwise scales. We also examine structural differences between steady-state covariance matrices that result from local and global analyses. We provide an explanation for the origin of such disparity using the 2D diffusion equation. Our ongoing effort is directed at finding a mathematically rigorous explanation for the cascade of periodic structures and their ordering across the spectrum of the steady-state velocity covariance matrix.

References

[1] P. J. Schmid and D. S. Henningson, *Stability and Transition in Shear Flows*. New York: Springer-Verlag, 2001.

[2] P. J. Schmid, "Nonmodal stability theory," *Annu. Rev. Fluid Mech.*, vol. 39, pp. 129–162, 2007.

[3] B. F. Farrell and P. J. Ioannou, "Stochastic forcing of the linearized Navier-Stokes equations," *Phys. Fluids A*, vol. 5, no. 11, pp. 2600–2609, 1993.

[4] B. Bamieh and M. Dahleh, "Energy amplification in channel flows with stochastic excitation," *Phys. Fluids*, vol. 13, no. 11, pp. 3258–3269, 2001.

[5] M. R. Jovanović and B. Bamieh, "Componentwise energy amplification in channel flows," *J. Fluid Mech.*, vol. 534, pp. 145–183, 2005.

[6] Y. Hwang and C. Cossu, "Linear non-normal energy amplification of harmonic and stochastic forcing in the turbulent channel flow," *J. Fluid Mech.*, vol. 664, pp. 51–73, 2010.

[7] R. Moarref and M. R. Jovanović, "Model-based design of transverse wall oscillations for turbulent drag reduction," *J. Fluid Mech.*, vol. 707, pp. 205–240, September 2012.

[8] A. Zare, M. R. Jovanović, and T. T. Georgiou, "Colour of turbulence," *J. Fluid Mech.*, vol. 812, pp. 636–680, February 2017.

[9] T. Herbert, "Secondary instability of boundary layers," *Ann. Rev. Fluid Mech.*, vol. 20, pp. 487–526, 1988.

[10] T. Herbert, "Parabolized stability equations," *Annu. Rev. Fluid Mech.*, vol. 29, no. 1, pp. 245–283, 1997.

[11] W. Ran, A. Zare, M. J. P. Hack, and M. R. Jovanović, "Modeling mode interactions in boundary layer flows via Parabolized Floquet Equations," *Phys. Rev. Fluids*, vol. 4, no. 2, p. 023901, February 2019.

[12] U. Ehrenstein and F. Gallaire, "On two-dimensional temporal modes in spatially evolving open flows: the flat-plate boundary layer," *J. Fluid Mech.*, vol. 536, pp. 209–218, 2005.

[13] J. W. Nichols and S. K. Lele, "Global modes and transient response of a cold supersonic jet," *J. Fluid Mech.*, vol. 669, pp. 225–241, 2011.

[14] A. Monokrousos, E. Åkervik, L. Brandt, and D. S. Henningson, "Global three-dimensional optimal disturbances in the blasius boundary-layer flow using time-steppers," *J. Fluid Mech.*, vol. 650, pp. 181–214, 2010.

[15] J. Jeun, J. W. Nichols, and M. R. Jovanović, "Input-output analysis of high-speed axisymmetric isothermal jet noise," *Phys. Fluids*, vol. 28, no. 4, p. 047101 (20 pages), April 2016.

[16] O. T. Schmidt, A. Towne, G. Rigas, T. Colonius, and G. A. Brès, "Spectral analysis of jet turbulence," *J. Fluid Mech.*, vol. 855, pp. 953–982, 2018.

[17] W. Ran, A. Zare, M. J. P. Hack, and M. R. Jovanović, "Stochastic receptivity analysis of boundary layer flow," *Phys. Rev. Fluids*, 2018, submitted; also arXiv:1807.07759.

[18] J. A. C. Weideman and S. C. Reddy, "A MATLAB differentiation matrix suite," *ACM Trans. Math. Software*, vol. 26, no. 4, pp. 465–519, December 2000.

[19] F. Alizard and J. Robinet, "Spatially convective global modes in a boundary layer," *Phys. Fluids*, vol. 19, no. 11, p. 114105, 2007.

[20] A. Mani, "Analysis and optimization of numerical sponge layers as a nonreflective boundary treatment," *J. Comput. Phys.*, vol. 231, no. 2, pp. 704–716, 2012.

[21] W. Ran, A. Zare, J. W. Nichols, and M. R. Jovanović, "The effect of sponge layers on global stability analysis of Blasius boundary layer flow," in *Proceedings of the 47th AIAA Fluid Dynamics Conference*, 2017, pp. 3456–3467.

[22] J. M. Kendall, "Experiments on boundary-layer receptivity to free-stream turbulence," *AIAA Paper*, p. 530, 1998.

[23] M. Matsubara and P. H. Alfredsson, "Disturbance growth in boundary layers subjected to free-stream turbulence," *J. Fluid Mech.*, vol. 430, pp. 149–168, 2001.

[24] P. Luchini, "Reynolds-number-independent instability of the boundary layer over a flat surface: optimal perturbations," *J. Fluid Mech.*, vol. 404, pp. 289–309, 2000.

[25] P. Andersson, M. Berggren, and D. Henningson, "Optimal disturbances and bypass transition in boundary layers," *Phys. Fluids*, vol. 11, no. 1, pp. 134–150, 1999.

[26] M. J. P. Hack and T. A. Zaki, "Modal and non-modal stability of boundary layers forced by spanwise wall oscillations," *J. Fluids Mech.*, vol. 778, pp. 389–427, 2015.

[27] M. J. P. Hack and P. Moin, "Algebraic disturbance growth by interaction of Orr and lift-up mechanisms," *J. Fluid Mech.*, vol. 829, pp. 112–126, 2017.